Electrochemical rejuvenation of anodically coloring electrochromic nickel oxide thin films

Hui-Ying Qu[a,b], Daniel Primetzhofer[c], Miguel A. Arvizu[a], Zhen Qiu[a], Umut Cindemir[a], Claes G. Granqvist[a], and Gunnar A. Niklasson[a]*

[a] Department of Engineering Sciences, The Ångström Laboratory, Uppsala University, SE-75120 Uppsala, Sweden

[b] MIIT Key Laboratory of Critical Materials Technology for New Energy Conversion and Storage, School of Chemistry and Chemical Engineering, Harbin Institute of Technology,150001 Harbin, China

[c] Department of Physics and Astronomy, The Ångström Laboratory, Uppsala University, SE-75120 Uppsala, Sweden

KEYWORDS: Electrochromism, nickel oxide, thin film, electrochemical rejuvenation, ToF-ERDA

ABSTRACT: Nickel oxide thin films are of major importance as anodically coloring components in electrochromic smart windows with applications in energy-efficient buildings. However, the optical performance of these films degrades upon extended electrochemical cycling, which has hampered their implementation. Here, we use a potentiostatic treatment to rejuvenate degraded nickel oxide thin films immersed in electrolyte of $LiClO_4$ in propylene carbonate. Time-of-flight elastic recoil detection analysis provided unambiguous evidence that both Li^+ ions and Cl-based ions participate in the rejuvenation process. Our work provides new perspectives for developing ion-exchange-based devices embodying nickel oxide.

……..

*E-mail: Gunnar.Niklasson@angstrom.uu.se

Electrochromic (EC) materials are able to change their optical properties upon the application of a small electrical signal.[1,2] There are two main classes of EC oxides, conventionally referred to as cathodic (coloring under ion insertion) and anodic (coloring under ion extraction). Optically efficient thin-film EC devices for transmittance modulation can be prepared as five-layer structures with a central ion conductor (electrolyte) joining one cathodically coloring film and another anodically coloring film; these layers are positioned between transparent electrical conductors, and the entire arrangement is backed by a transparent substrate or located between two such substrates.[2,3] Thin-film EC devices have numerous applications in current and forthcoming technology, the largest—at least as regards surface areas—being in smart glazing (windows and glass facades) for energy-efficient buildings with good indoor comfort.[3] The majority of EC-based smart glazing in use today (2017) involves cathodic tungsten-oxide-based and anodic nickel-oxide-based thin films prepared by reactive dc magnetron sputtering.[3,4]

Most EC devices must be durable for extended periods of time, and this is especially so for smart glazing which should last for decades and be able to sustain tens of thousands of transmittance modulation cycles. EC devices, as any ion-exchange-based construction, tend to lose their performance over time, and it is not surprising that extensive studies have been conducted in order to improve EC materials; these efforts have included the use of doping elements,[5–8] nanostructural modification,[9–11] and formation of composites with other materials.[12,13] Nevertheless, there has remained an urgent need for other means to extend device longevity, and it was recently shown that electrochemical treatments can rejuvenate degraded EC films and restore their original properties. This work was initiated with WO_3 films[14–18] and was later extended to films of MoO_3[19] and TiO_2.[20] These oxides are cathodic and similar in many ways, and it is commonly accepted that their electrochromism is associated with the intercalation/deintercalation of small cations (H^+ or Li^+) and concurrent insertion/extraction of electrons. Rejuvenation of WO_3 has been firmly related to electrically induced extraction of trapped Li^+ ions from degraded films.[14,15,18] However, the situation is more complex for the case of anodically coloring nickel oxide in the Li^+-based electrolytes.[21–23] Its coloration mechanism remains contentious and even the ionic species involved in the EC process are controversial, furthermore, the physical and chemical origins of the films' irreversibility remain obscure, experimentally as well as theoretically. It was previously shown that the transmittance contrast of a degraded $Ni(OH)_2$ film cycled in KOH could be restored by an annealing treatment.[24] But since nickel oxide films are widely used with Li^+-containing electrolytes in EC glazing, as noted above, it is of large importance to find out whether they also can be rejuvenated. As reported in the present Letter, this is indeed the case.

EC nickel oxide thin films were prepared by reactive DC magnetron sputtering onto glass substrates pre-coated with transparent and electrically conducting layers of In_2O_3:Sn (known as ITO) as detailed in the Supporting Information (SI). Films with thicknesses of about 300 nm were crystalline and had cubic fcc structure, as indicated by X-ray diffraction patterns (Figure S1); these results are consistent with findings in prior work.[23] Elemental compositions were determined by Rutherford Backscattering Spectrometry (RBS) (Figure S2). Data indicated the presence of nickel and oxygen in addition to some contribution at least partially due to the carbon substrate used for RBS. The film composition was consistent with $NiO_{1.15}$; the statistical uncertainty was ±0.04 as inferred from peak heights in the RBS spectra. Oxygen

over-stoichiometry is consistent with prior results.[23] The film density was found to be 4.32 g cm^{-3} by relating RBS data to surface profilometry results. This value is far less than that expected for bulk NiO (6.67 g cm^{-3}) and indicates that our films are porous. Direct evidence for porosity was obtained by scanning electron microscopy (SEM), and the image in Figure 1 exhibits nanostructure on the scale of ~25 nm as well as cracks and crevices separated by some 200–400 nm. Time-of Flight Elastic Recoil Detection Analysis (ToF-ERDA) was carried out to supplement the RBS recordings and in order to measure elemental concentrations in nickel oxide films without recourse to standards and with emphasis on light species (see SI for details). The concentrations of nickel and oxygen were found to be ~45 and ~51 at.%, respectively, thus indicating that the ToF-ERDA data were consistent with those taken by RBS. The as-deposited film was visibly brownish, which is in agreement with earlier observations on oxygen-rich nickel oxide films.[23]

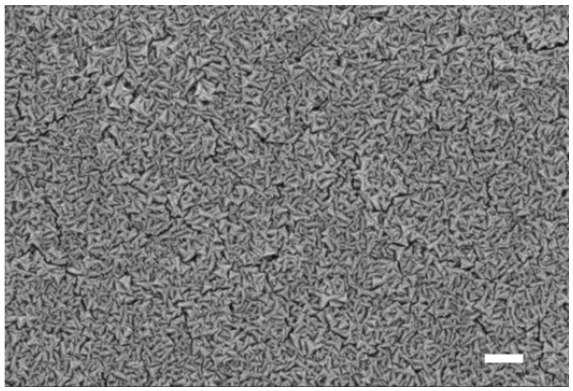

Figure 1. SEM image of a ~300-nm-thick as-deposited $NiO_{1.15}$ film. The scale bar is 200 nm.

Cyclic voltammetry (CV) data were recorded in an argon-filled glove box using a three-electrode electrochemical cell. The EC film served as working electrode and was electrochemically cycled in an electrolyte of 1 M $LiClO_4$ dissolved in propylene carbonate (PC). The counter and reference electrodes consisted of Li foil. The voltage scan rate was 50 mV s^{-1}. All CV measurements started from the open circuit potential, and all voltages reported here refer to a Li/Li^+ reference. Optical transmittance in the wavelength range 400–800 nm was monitored by *in situ* measurements.

CV recordings within a conventional voltage range of 2.0–4.0 V led to significant degradation of the $NiO_{1.15}$ film, as seen in Figure 2(a). The charge capacity, given by the encircled area in the CV data, decreased upon extended cycling and was greatly reduced after the 500^{th} cycle. The shrinking was monotonic for both coloration and bleaching, as evident from Figure 2(b), and the charge capacity during coloration was larger than that during bleaching, except for the first CV cycle. Expectedly, the decreased charge capacity led to smaller optical modulation and, in particular the colored state was degraded while the bleached-state transmittance remained unaltered (upper inset in Figure 2c). During the degradation process, the coloration efficiency of the $NiO_{1.15}$ film decreased from an initial value of 51.4 cm^2 C^{-1} to 23.3 cm^2 C^{-1} after 500 cycles. There was no apparent change of film morphology upon degradation, as seen from the SEM image in Figure S3(a). Our present

results are in line with a previous study of the potential dependence of the degradation process.[25]

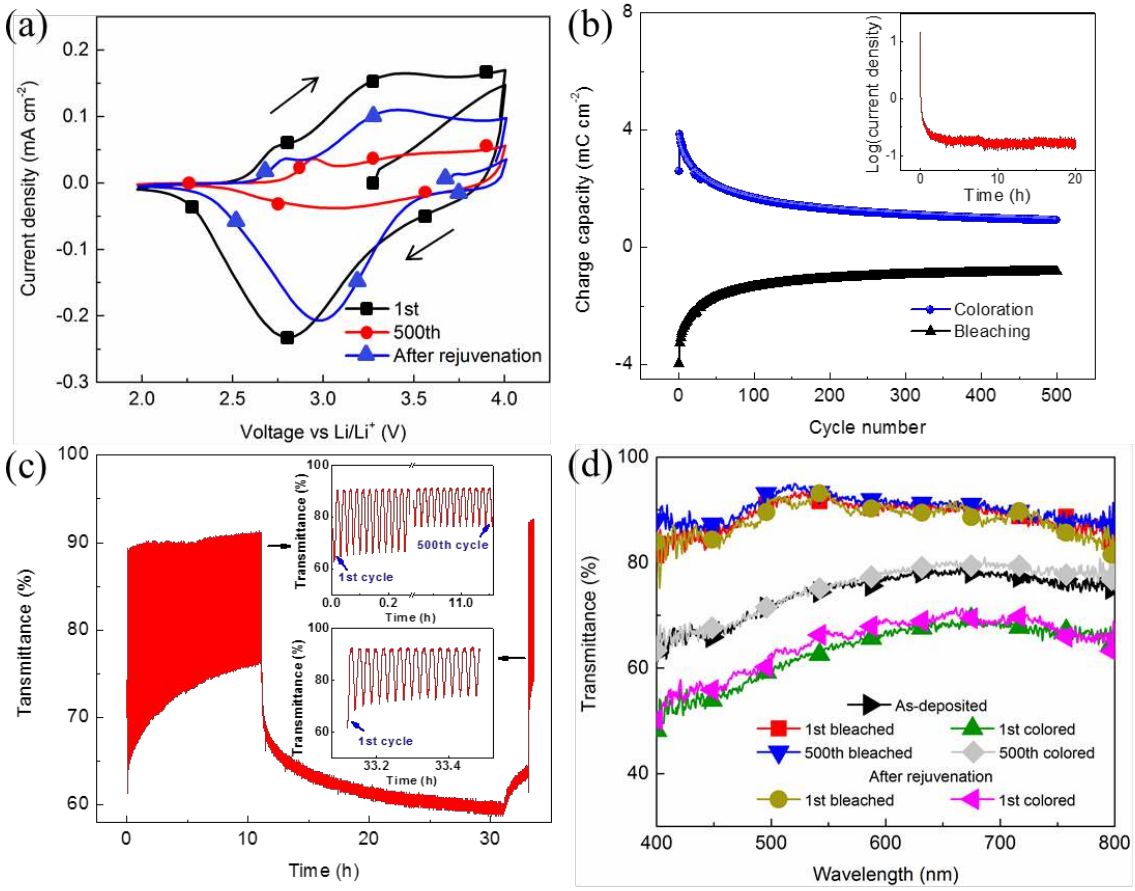

Figure 2. Electrochemical and EC performance of ~300-nm-thick $NiO_{1.15}$ films. (a) CV data recorded at a voltage scan rate of 50 mV s^{-1} after the indicated numbers of cycles and subsequent to rejuvenation; arrows indicate voltage sweep direction. (b) Charge capacity degradation during 500 consecutive CV cycles; insert shows log(current density) *versus* time during potentiostatic rejuvenation at a constant potential of 4.1 V (current density is in units of μA cm^{-2}). (c) *In situ* optical transmittance at a mid-luminous wavelength of 550 nm upon electrochemical treatments; the electrochemical operations were as follows: (*i*) 500 CV cycles were run in the range of 2.0–4.0 V at a scan rate of 50 mV s^{-1} (with time-resolved data displayed in the upper inset), (*ii*) potentiostatic rejuvenation was subsequently performed for 20 h at a potential of 4.1 V followed by a resting period of 2 h and, finally, (*iii*) several CV cycles were run as in (*i*) (with time-resolved data displayed in the lower inset). (d) *In situ* spectral optical transmittance in the 400–800 nm wavelength range after CV cycling in the range of 2.0–4.0 V at a scan rate of 50 mV s^{-1}; data are shown for the as-deposited state, after treatment for the stated number of cycles, and subsequent to rejuvenation (some curves are partly overlapping).

A potentiostatic technique was used to rejuvenate the degraded $NiO_{1.15}$ film, specifically applying a constant potential of 4.1 V during a 20-h period after the electrochemical cycling. The CV data in Figure 2(a) show that the film then regains most of its initial charge capacity, which demonstrates the key finding of our work: that electrochemical rejuvenation is possible for anodically coloring EC films of nickel oxide. No noticeable change of the film morphology was connected with the rejuvenation (Figure S3b). A degraded sample left in the

electrolyte for 20 h without any applied bias did not exhibit any rejuvenation of its electrochromic properties (Figure S4).

Rejuvenation was further verified by *in situ* optical transmittance measurements, as illustrated in Figure 2(c). When a constant potential of 4.1 V was applied, the optical transmittance at a wavelength of 550 nm dropped monotonically during the entire rejuvenation process; the change was very fast at the beginning, but the decrease then became more gradual and eventually the film reached a transmittance value similar to that of the initial colored film. The associated current density evolution (inset in Figure 2b) indicates an abrupt decrease in current density at the beginning of the rejuvenation. A charge of 5.46 mC cm^{-2} was calculated from current density *versus* time; this value is qualitatively similar, but not equal to, the charge capacity difference between the first and 500^{th} cycle during the CV measurement (2.69 mC cm^{-2}). Figure 2(d) shows spectral optical transmittance in the visible wavelength range for as-deposited, degraded, and rejuvenated films. The initial large optical contrast between bleached and colored states decreased rapidly upon CV cycling in the potential range of 2.0–4.0 V, and the colored state transmittance eventually approached that of the as-deposited film. However, the original colored-state transmittance was recovered after completion of the rejuvenation process. In addition, the coloration efficiency regained its initial value. Clearly, the rejuvenated $NiO_{1.15}$ film displayed approximately the same EC performance as that in the initial state during the first CV cycle after the rejuvenation.

However, there were some minor but noteworthy differences in the areas and shapes of the cyclic voltammograms recorded in the first CV cycle during film degradation and in the first CV cycle after rejuvenation, and there were also variations in the open circuit potentials which changed correspondingly from ~3.3 to ~3.7 V as indicated by the starting potentials of the respective CV curves (Figure 2a). In addition, although the rejuvenated $NiO_{1.15}$ film displayed virtually the same properties as those of the as-deposited film during the first CV cycle, the rejuvenated film showed more rapid degradation from the second cycle onwards, as apparent from a comparison of the optical transmittance modulation recorded during the first few CV cycles (insets in Figure 2c).

ToF-ERDA measurements were carried out in order to elucidate the nature of the ion species involved in the film degradation and rejuvenation. Elemental depth profiling of atomic concentrations was accomplished for three $NiO_{1.15}$-based films corresponding to different stages of the CV cycling–rejuvenation process: after one CV cycle, after 500 cycles (strongly degraded film), and after rejuvenation. The analyzed films were in the shown states. Figure 3(a) shows elemental depth profiles for the heavily degraded film, and Figure 3(b) presents part of its recorded time-of-flight/energy coincidence spectrum. The data provide clear evidence for significant concentrations of the expected elements (Ni, O, Li, and H) throughout the cross-sections of the films. There are unambiguous data indicating carbon contamination probably ensuing from the sputter deposition. Signals from Na, Si, Ca, and In originate from the ITO-coated substrate; their appearance is believed to be associated with pronounced porosity as well as with cracks in the films (Figures 1 and S3) that are aggravated by ion bombardment inherent in the ToF-ERDA recordings (Figure S5). A minor amount of a contamination with mass ~80 may be due to the glass substrate. The concentration of this impurity did not change during the rejuvenation process. It is particularly interesting to note that Cl is detected in cycled, degraded and rejuvenated nickel oxide films. The Cl species

cannot be ascertained; for example the added oxygen in adsorbed ClO_4^- ions would be too small, in comparison to the oxygen in $NiO_{1.15}$, to be distinguished. The small concentrations of Li and Cl are in line with the low charge capacity recorded during the CV cycling. Table 1 reports concentrations of the most significant elements for $NiO_{1.15}$-based films studied by ToF-ERDA; the data represent averages across a depth of 1500×10^{15} atoms cm^{-2}.

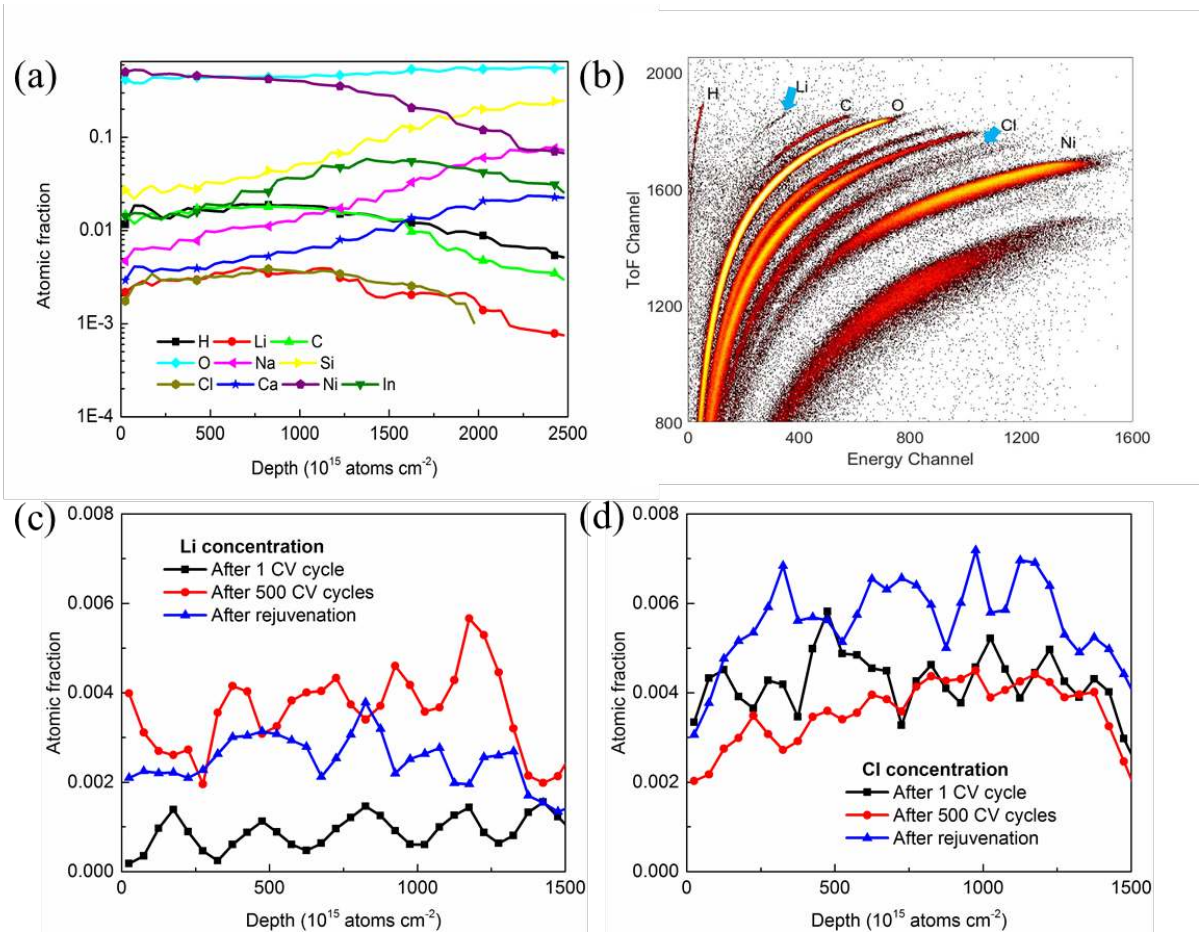

Figure 3. ToF-ERDA data for ~300-nm-thick $NiO_{1.15}$ films. A film thickness of 300 nm corresponds to approximately 1500×10^{15} atoms cm^{-2}. (a) Depth profiles for the shown elements in a severely degraded film subjected to 500 CV cycles in the potential range of 2.0−4.0 V. (b) Time-of-flight/energy coincidence spectrum from which the information in (a) was acquired; data were recorded for 36 MeV $^{127}I^{8+}$ primary ions and refer to the indicated elements. (c)–(d) Depth profiles for Li and Cl recorded on films in the colored state subjected to the indicated treatments; data are indicated by symbols, which were joined by straight lines for convenience.

Table 1. Elemental concentrations for ~300-nm-thick $NiO_{1.15}$ films in the shown states after the indicated electrochemical treatments.

Film treatment	Element contents in at.%				
	Li	Cl	Ni	O	H
After 1 CV cycle, bleached	1.06	0.16	46.5	48.0	2.0
After 1 CV cycle, colored	0.09	0.43	45.6	49.3	2.1
After 500 CV cycles, colored	0.36	0.36	46.0	49.1	1.9
After rejuvenation, colored	0.25	0.57	46.3	48.1	2.0

The depth profiles of Li and Cl are particularly interesting and are shown in detail in Figures 3(c) and 3(d), respectively, for the variously treated films in the colored state. After the first CV cycle, the Li concentration was as small as 0.09 at.% while the Cl content attained the comparatively high value of 0.43 at.%. The difference in atomic contents may be attributed to Cl-based anions being attracted to the film by electromagnetic force under a potential of 4.1 V while Li^+ ions were concurrently repelled. However, after 500 CV cycles the Li content went up to 0.36 at.%, which is the same concentration as observed for Cl. These results highlight that the electrochromism of nickel oxide embodies a combination of Li^+ cation removal/accumulation and Cl-based anion accumulation/removal. Supporting evidence for this mechanism comes from ToF-ERDA measurements in colored and bleached states during the first cycle (Table 1). It is clearly seen that the Li content is higher in the bleached state and the Cl content is higher in the colored state. Potentiostatic rejuvenation subsequently decreased the Li concentration to 0.25 at.%, thus demonstrating successful removal of Li^+ ions, as compared to the degraded film, while it raised the Cl concentration to 0.57 at.%. It should be noted that Li and Cl were detected throughout the films' depths, which probably implies that Li^+ and Cl-based ions adsorb at pore surfaces and in cracks and crevices in the film. The concentration of H remained almost unaltered during the various treatments, thus indicating that protons and/or OH^- groups adsorbed on the surface of the as-deposited film do not play any significant role for the EC properties of the $NiO_{1.15}$ films. The ToF-ERDA data can be summarized as follows: (*i*) Accumulation of Li^+ and Cl-based ions take place throughout the cross-section of an EC $NiO_{1.15}$-based film in an electrolyte of $LiClO_4$ in PC, (*ii*) degradation of the $NiO_{1.15}$ film under voltammetric cycling is associated with further accumulation of Li^+ and removal of Cl-based ions, and (*iii*) potentiostatic rejuvenation of the degraded $NiO_{1.15}$ film is a collective effect of removal of Li^+ ions and accumulation of Cl-based ions.

In conclusion, severely degraded nickel oxide thin films are able to regain their initial EC performance by potentiostatic rejuvenation in an electrolyte of $LiClO_4$ in PC. This process involves a collective effect of removal of Li^+ ions and accumulation of Cl-based ions. Furthermore, our work provided new and significant information on the electrochromism of nickel oxide in contact with Li^+-conducting electrolytes, which thus far has been an elusive topic and subject to speculations for many years. The new insights may be useful for understanding and evading ageing and degradation of EC devices incorporating anodically coloring nickel oxide, which is a crucial issue for smart windows and glass facades in energy efficient buildings with superior indoor comfort. Our new results are possibly applicable also to other types of nickel-oxide-based ionic devices such as batteries and supercapacitors.

Associated content:

Supporting Information.

Acknowledgement:

Hui-Ying Qu is grateful for financial support from the China Scholarship Council Doctoral Joint-Training Program.

References:

(1) Granqvist, C. G. *Handbook of Inorganic Electrochromic Materials*; Elsevier: Amsterdam, the Netherlands, 1995.

(2) Mortimer, R. J.; Rosseinsky, D. R.; Monk, P. M. S., Eds. *Electrochromic Materials and Devices*; Wiley-VCH: Weinheim, Germany, 2015.

(3) Granqvist, C. G. Electrochromics for Smart Windows: Oxide-Based Thin Films and Devices. *Thin Solid Films* **2014**, *564*, 1–38.

(4) Niklasson, G. A.; Granqvist, C. G. Electrochromics for Smart Windows: Thin Films of Tungsten Oxide and Nickel Oxide, and Devices Based on These. *J. Mater. Chem.* **2007**, *17*, 127–156.

(5) Lin, F.; Nordlund, D.; Weng, T.-C.; Moore, R. G.; Gillaspie, D. T.; Dillon, A. C.; Richards, R. M.; Engtrakul, C. Hole Doping in Al-Containing Nickel Oxide Materials to Improve Electrochromic Performance. *ACS Appl. Mater. Interfaces* **2013**, *5*, 301–309.

(6) Lu, Y.; Liu, L.; Mandler, D.; Lee, P. S. High Switching Speed and Coloration Efficiency of Titanium-Doped Vanadium Oxide Thin Film Electrochromic Devices. *J. Mater. Chem. C* **2013**, *1*, 7380–7386.

(7) Wen, R.-T.; Niklasson, G. A.; Granqvist, C. G. Strongly Improved Electrochemical Cycling Durability by Adding Iridium to Electrochromic Nickel Oxide Films. *ACS Appl. Mater. Interfaces* **2015**, *7*, 9319–9322.

(8) Arvizu, M. A.; Niklasson, G. A.; Granqvist, C. G. Electrochromic $W_{1-x-y}Ti_xMo_yO_3$ Thin Films Made by Sputter Deposition: Large Optical Modulation, Good Cycling Durability, and Approximate Color Neutrality. *Chem. Mater.* **2017**, *29*, 2246–2253.

(9) Yang, L.; Ge, D.; Zhao, J.; Ding, Y.; Kong, X.; Li, Y. Improved Electrochromic Performance of Ordered Macroporous Tungsten Oxide Films for IR Electrochromic Device. *Sol. Energy Mater. Sol. Cells* **2012**, *100*, 251–257.

(10) Scherer, M. R. J.; Steiner, U. Efficient Electrochromic Devices Made from 3D Nanotubular Gyroid Networks. *Nano Lett.* **2013**, *13*, 3005–3010.

(11) Liang, L.; Zhang, J.; Zhou, Y.; Xie, J.; Zhang, X.; Guan, M.; Pan, B.; Xie, Y. High-Performance Flexible Electrochromic Device Based on Facile Semiconductor-to-Metal Transition Realized by $WO_3 \cdot 2H_2O$ Ultrathin Nanosheets. *Sci. Rep.* **2013**, *3*, 1936/1–1936/8.

(12) Cai, G.-F.; Tu, J.-P.; Zhang, J.; Mai, Y.-J.; Lu, Y.; Gu, C.-D.; Wang, X.-L. An Efficient Route to a Porous NiO/Reduced Graphene Oxide Hybrid Film with Highly Improved Electrochromic Properties. *Nanoscale* **2012**, *4*, 5724–5730.

(13) Qu, H.; Zhang, X.; Zhang, H.; Tian, Y.; Li, N.; Lv, H.; Hou, S.; Li, X.; Zhao, J.; Li, Y. Highly Robust and Flexible $WO_3 \cdot 2H_2O$/PEDOT Films for Improved Electrochromic Performance in Near-Infrared Region. *Sol. Energy Mater. Sol. Cells* **2017**, *163*, 23–30.

(14) Wen, R.-T.; Granqvist, C. G.; Niklasson, G. A. Eliminating Degradation and Uncovering Ion-Trapping Dynamics in Electrochromic WO_3 Thin Films. *Nat. Mater*. **2015**, *14*, 996–1001.

(15) Arvizu, M. A.; Wen, R.-T.; Primetzhofer, D.; Klemberg-Sapieha, J. E.; Martinu, L.; Niklasson, G. A.; Granqvist, C. G. Galvanostatic Ion Detrapping Rejuvenates Oxide Thin Films. *ACS Appl. Mater. Interfaces* **2015**, *7*, 26387–26390.

(16) Wen, R.-T.; Niklasson, G. A.; Granqvist, C. G. Sustainable Rejuvenation of Electrochromic WO_3 Films. *ACS Appl. Mater. Interfaces* **2015**, *7*, 28100–28104.

(17) Wen, R.-T.; Arvizu, M. A.; Morales-Luna, M.; Granqvist, C. G.; Niklasson, G. A. Ion Trapping and Detrapping in Amorphous Tungsten Oxide Thin Films Observed by Real-Time Electro-Optical Monitoring. *Chem. Mater*. **2016**, *28*, 4670–4676.

(18) Baloukas, B.; Arvizu, M. A.; Wen, R.-T.; Niklasson, G. A.; Granqvist, C. G.; Vernhes, R.; Klemberg-Sapieha, J. E.; Martinu, L. Galvanostatic Rejuvenation of Electrochromic WO_3 Thin Films: Ion Trapping and Detrapping Observed by Optical Measurements and by Time-of-Flight Secondary Ion Mass Spectrometry. *ACS Appl. Mater. Interfaces* **2017**, *9*, 16995–17001.

(19) Arvizu, M. A.; Granqvist, C. G.; Niklasson, G. A. Rejuvenation of Degraded Electrochromic MoO_3 Thin Films Made by DC Magnetron Sputtering: Preliminary Results. *J. Phys.: Conf. Ser*. **2016**, *764*, 012009/1–012009/6.

(20) Wen, R.-T.; Niklasson, G. A.; Granqvist, C. G. Eliminating Electrochromic Degradation in Amorphous TiO_2 through Li-Ion Detrapping. *ACS Appl. Mater. Interfaces* **2016**, *8*, 5777–5782.

(21) Boschloo, G.; Hagfeldt, A. Spectroelectrochemistry of Nanostructured NiO. *J. Phys. Chem. B* **2001**, *105*, 3039–3044.

(22) Mikhelčič, M.; Šurca Vuk, A.; Jerman, I.; Orel, B.; Švegel, F.; Moulki, H.; Faure, C.; Campet, G.; Rougier, A. Comparison of Electrochromic Properties of $Ni_{1-x}O$ in Lithium and Lithium-Free Aprotic Electrolytes: From $Ni_{1-x}O$ Pigment Coatings to Flexible Electrochromic Devices. *Sol. Energy Mater. Sol. Cells* **2014**, *120*, 116–130.

(23) Wen, R.-T.; Granqvist, C. G.; Niklasson, G. A. Anodic Electrochromism for Energy-Efficient Windows: Cation/Anion-Based Surface Processes and Effects of Crystal Facets in Nickel Oxide Thin Films. *Adv. Funct. Mater*. **2015**, *25*, 3359–3370.

(24) Ren, Y.; Chim, W. K.; Guo, L.; Tanoto, H.; Pan, J.; Chiam, S. Y. The Coloration and Degradation Mechanisms of Electrochromic Nickel Oxide. *Sol. Energy Mater. Sol. Cells* **2013**, *116*, 83–88.

(25) Wen, R.-T.; Granqvist, C. G.; Niklasson, G. A. Anodic Electrochromic Nickel Oxide Thin Films: Decay of Charge Density upon Extensive Electrochemical Cycling. *ChemElectroChem* **2016**, 3, 266-275.

TOC

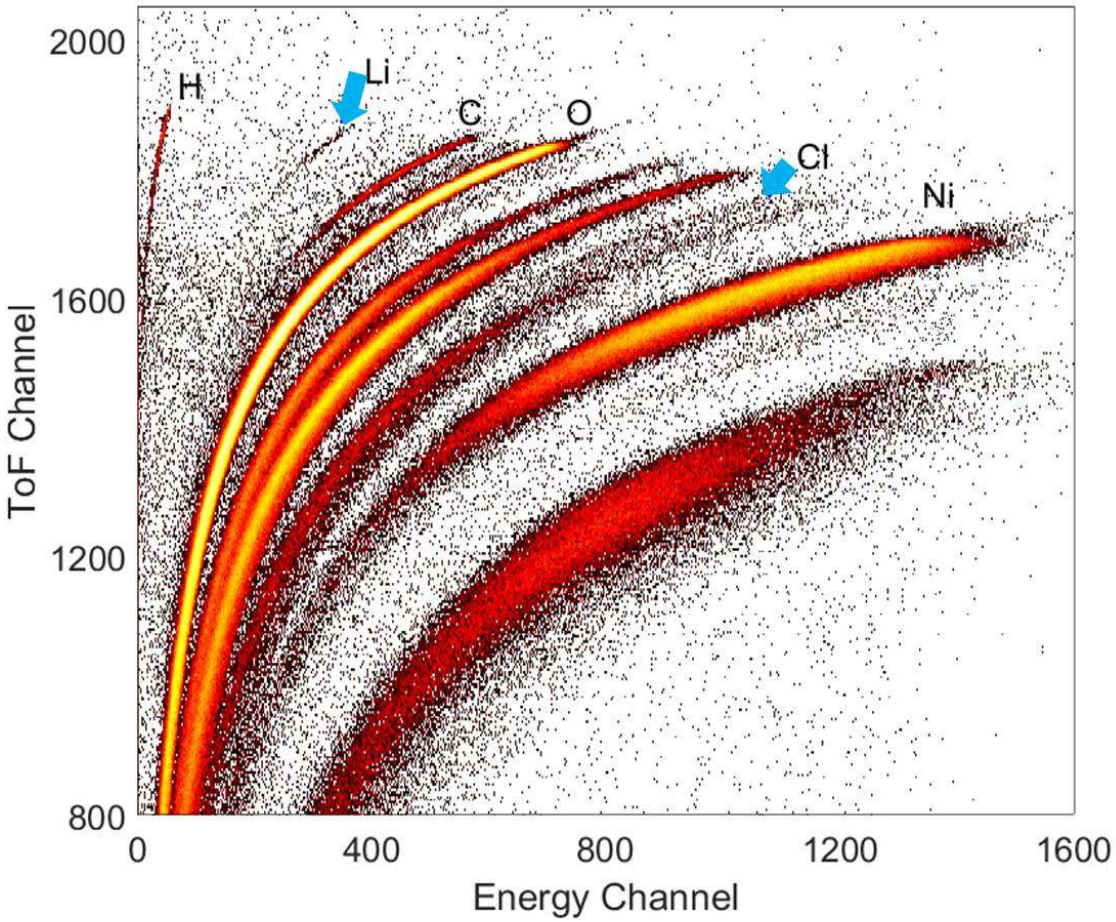
2000
1600
1200
800
ToF Channel
0
400
800
1200
1600
Energy Channel
H
Li
C
O
Cl
Ni

Supporting Information

Electrochemical rejuvenation of anodically coloring electrochromic nickel oxide thin films

Hui-Ying Qu[a,b], Daniel Primetzhofer[c], Miguel A. Arvizu[a], Zhen Qiu[a], Umut Cindemir[a], Claes G. Granqvist[a], and Gunnar A. Niklasson*[a]

[a] Department of Engineering Sciences, The Ångström Laboratory, Uppsala University, SE-75120 Uppsala, Sweden

[b] MIIT Key Laboratory of Critical Materials Technology for New Energy Conversion and Storage, School of Chemistry and Chemical Engineering, Harbin Institute of Technology,150001 Harbin, China

[c] Department of Physics and Astronomy, The Ångström Laboratory, Uppsala University, SE-75120 Uppsala, Sweden

*E-mail: Gunnar.Niklasson@angstrom.uu.se

Sample preparation and characterization

Nickel oxide thin films were deposited by reactive DC magnetron sputtering in a coating system based on a Balzers UTT 400 unit. The sputtering chamber contained 30 mTorr of argon and oxygen gas with the O_2/Ar ratio being 10%. These films were deposited onto unheated substrates of ITO-coated glass for EC measurements and simultaneously onto carbon plates for compositional analyses. The ITO layer had a sheet resistance of 60 Ω. Substrate rotation during sputter deposition ensured film uniformity. Film thicknesses were determined by surface profilometry using a Dektak XT instrument. Overall film morphology subsequent to ToF-ERDA measurements (see below) was observed with an Olympus BX60 optical microscope equipped with a 10× objective and a digital camera. More than 10 samples were prepared and investigated for the various kinds of measurements.

Film crystallinity was investigated by X-ray diffraction (XRD) using a Siemens D5000 instrument with CuK_α radiation at a wavelength of 0.154 nm. Structure and phase composition were obtained by comparison with the Joint Commission of Powder Diffraction Standards (JCPDS) database. XRD patterns (Figure S1) were consistent with crystalline nickel oxide with cubic fcc structure (JCDPS No. 47-1049), and diffraction peaks were assigned to the (111), (200), (220), (311), and (222) lattice planes. The peak heights decreased slightly during electrochemical treatments, from the as-deposited to the degraded and the rejuvenated film. Film morphology was characterized by Scanning Electron Microscopy (SEM) using a LEO 1550 FED Gemini instrument with an acceleration voltage of 10 kV. Nickel and oxygen contents were determined by Rutherford Backscattering Spectrometry (RBS) at the Uppsala Tandem Laboratory, using 2 MeV ^{4}He ions backscattered at an angle of 170°. RBS spectra (Figure S2) were fitted to a model for the film–substrate system by use of the SIMNRA program.[24]

Cyclic voltammetry (CV) was carried out in a conventional three-electrode cell by use of a computer-controlled ECO Autolab/GPES Interface. The whole measurement was conducted in an Ar-filled glove box with a water content of about 0.5 ppm. A $NiO_{1.15}$ film served as working electrode and was immersed in an electrolyte of 1 M $LiClO_4$ in PC. Both counter electrode and reference electrode were Li foils. Charge capacity C (mC cm^{-2}) was determined from CV data by

$$C = \int \frac{j dV}{s} \quad , \tag{S1}$$

where j is current density (mA cm^{-2}), s is scan rate (V s^{-1}), and V is voltage (V). Spectral optical transmittance was recorded *in situ* during electrochemical cycling; data were obtained by using a fiber optical instrument from Ocean Optics. The electrochemical cell was positioned between a tungsten halogen lamp and the detector, and a cell containing nothing but electrolyte was employed to obtain the 100-%-level for the transmittance; the calibration run was performed before inserting the sample in the electrolyte.

ToF-ERDA: Techniques and uncertainties

Time-of-Flight Elastic Recoil Detection Analysis (ToF-ERDA) was performed at the Tandem Accelerator Laboratory of Uppsala University in order to establish elemental depth-profiles of the constituent species of the nickel-oxide-based films. Before

measurements, the samples were washed with 1-propanol to remove any residual electrolyte. Two detection systems were employed during the study, with different detectors for energy discrimination of particles after the time-of-flight drift tube. Technical details of the set-ups can be found in the literature.[25,26]

Species identification was done via mass detection and permitted unambiguous assignments up to atomic numbers of about 20; for heavier nuclei, there were issues associated with limited resolution and with overlap due to isotope mass distributions. Absolute concentrations, independent of standards and without risks due to interference of signals originating from different species, were derived from time-of-flight/energy coincidence spectra (Figure 3b) by employing the software CONTES.[27]

In the present study, concentrations are subject to systematic uncertainties mainly originating from two sources. First, the time-of-flight detectors rely on electron emission from ultrathin free-standing carbon foils during ion transmission, which leads to detection efficiency deviating from unity in particular for light species. This efficiency can be as low as 40% in the case of Li—*i.e.*, for one of the most interesting elements in our study—but the employment of two different detection systems, as well as the possibility to execute absolute calibration by use of a pure element beam, renders this contribution to the systematic uncertainty to be 15–20% of the recorded concentrations for Li. Much smaller uncertainties pertain to other species of interest, such as Cl. Second, the specific energy loss of the primary ion in the material of interest, as well as the specific energy loss of recoiling nuclei from the target material, can contribute to uncertainties in recorded species concentrations; the maximum contribution from this source is on the order of 5–10% of the deduced concentration.

It should be noted that both types of systematic uncertainties will have equivalent impacts on concentrations in film targets of similar composition. This fact, in turn, means that relative concentrations, and changes in concentrations between different samples, can be determined independently of any influence of the systematic uncertainties and are predominantly governed by experiment statistics. These considerations can account for the observed scatter of the data for Li and Cl in Figures 3(c) and 3(d), respectively.

The ion bombardment inherent in ToF-ERDA measurements altered the film morphology (Figure S5) and led to the appearance of large-scale “waviness” presumably associated with cracks. This interpretation was supported by time-resolved analysis of ToF-ERDA data which showed increased signals due to the substrate upon extended beam exposure. However, the main purpose of ToF-ERDA recordings was to detect species responsible for the electrochromic effects, and hence this sample degradation is deemed to be of minor importance.

(26) Mayer, M. SIMNRA, a Simulation Program for the Analysis of NRA, RBS and ERDA. *AIP Conf. Proc*. **1999**, *475*, 541–544.

(27) Zhang, Y.; Whitlow, H. J.; Winzell, T.; Bubb, I. F.; Sajavaara, T.; Arstila, K.; Keinonen, J. Detection Efficiency of Time-of-Flight Energy Elastic Recoil Detection Analysis Systems. *Nucl. Instrum. Meth. Phys. Res. B* **1999**, *149*, 477–489.

(28) Ström, P.; Petersson, P.; Rubel, M.; Possnert, G. A Combined Segmented Anode Gas Ionization Chamber and Time-of-Flight Detector for Heavy Ion Elastic Recoil Detection Analysis. *Rev. Sci. Instr.* **2016**, *87*, 103303/1 – 103303/6.

(29) Janson, K. S. Internal Report 2004, Uppsala University, Sweden.

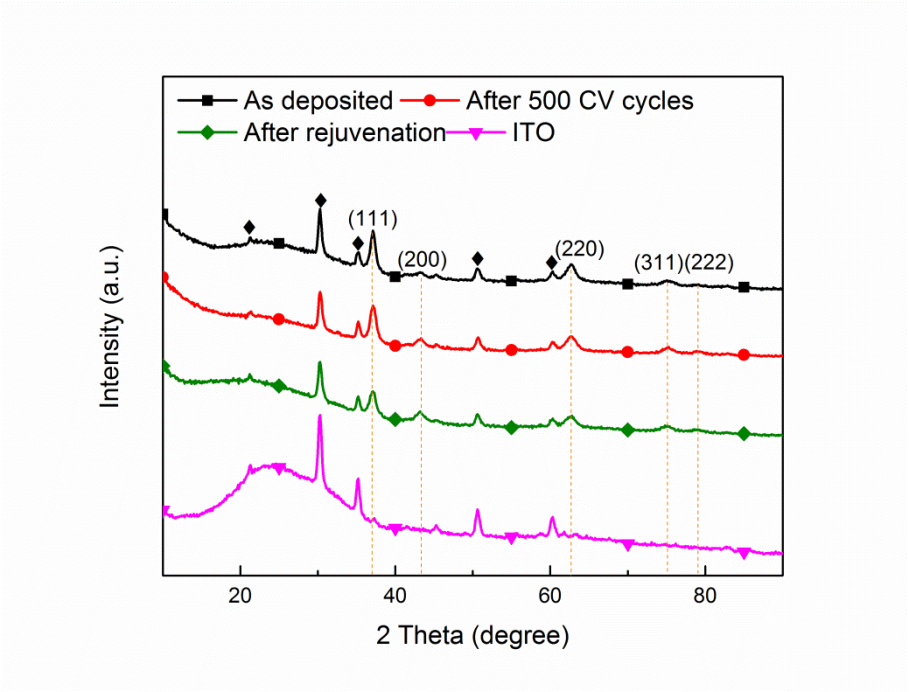

Figure S1. X-ray diffractograms recorded for a ~300-nm-thick $NiO_{1.15}$ film in the colored state backed by ITO-coated glass and subjected to the shown treatments. Data are reported also for a bare ITO-coated glass substrate. Diamonds mark the positions of the reflections due to ITO. Vertical dashed lines mark the expected positions of the stated reflections in NiO (JCDPS No. 47-1049).

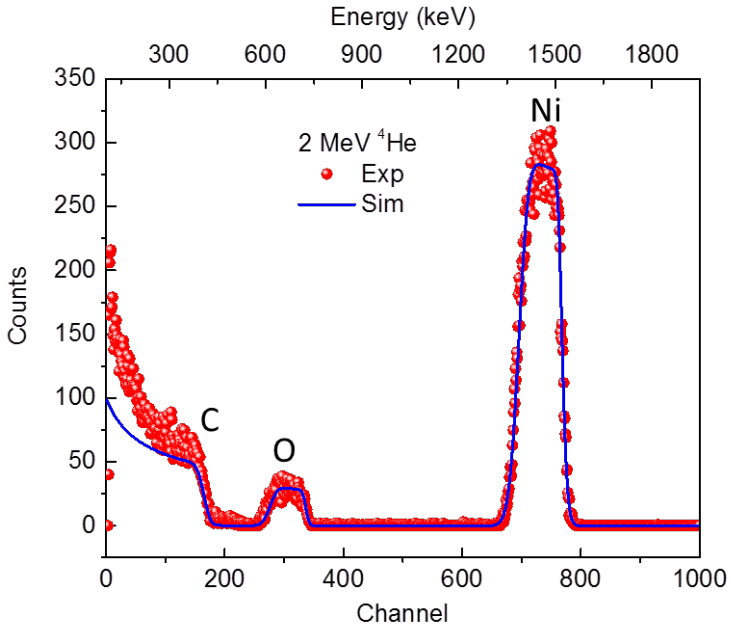

Figure S2. Experimental (Exp) and simulated (Sim) RBS spectra for a ~300-nm-thick $NiO_{1.15}$ film backed by carbon. Elemental compositions were determined by fitting experimental results (red dots) to simulated data (blue curve).

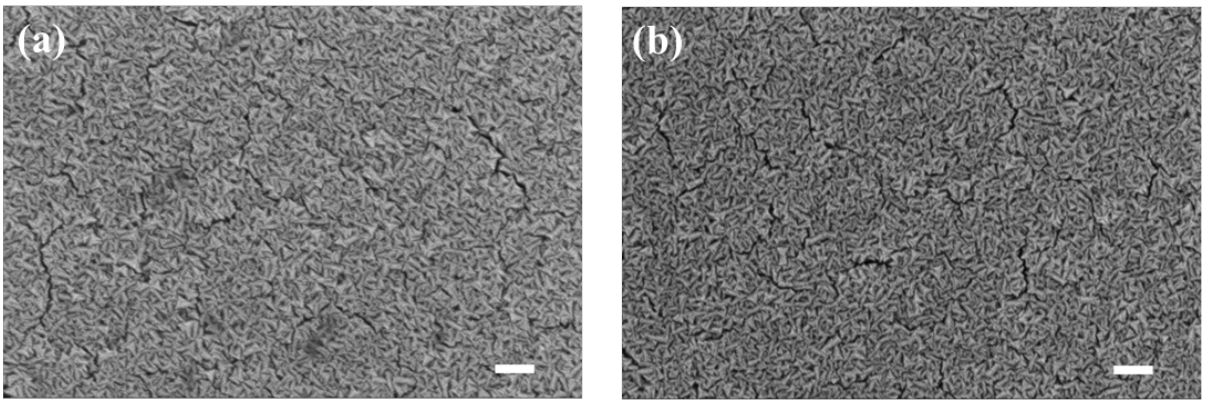

Figure S3. SEM images of ~300-nm-thick $NiO_{1.15}$ films (a) after being subjected to 500 CV cycles and thereby severely degraded and (b) after electrochemical rejuvenation. The scale bar is 200 nm.

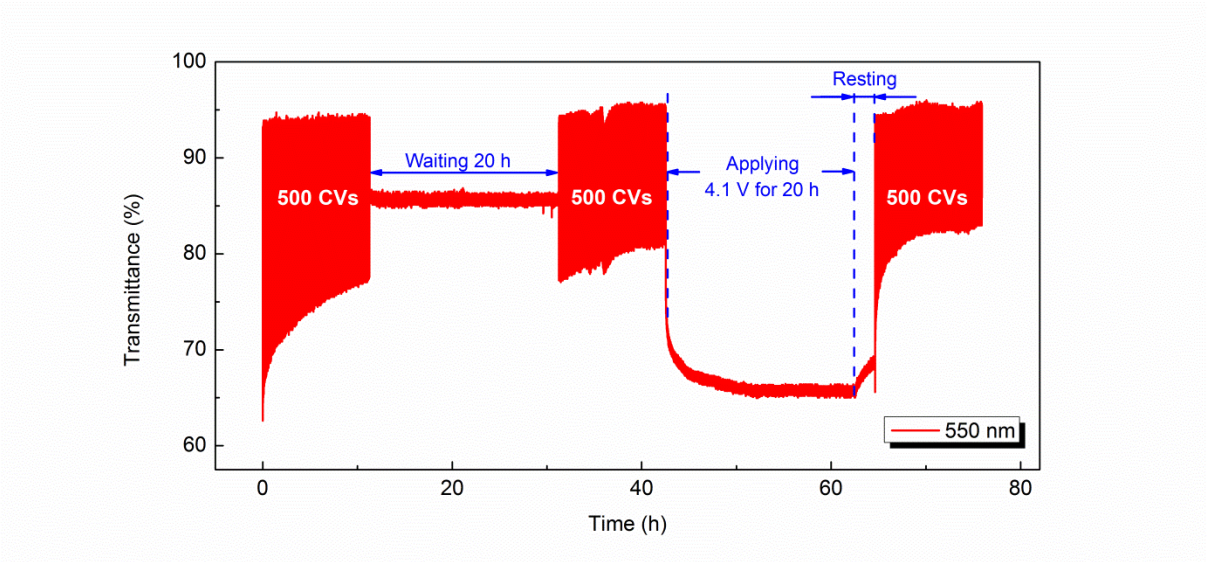

Figure S4. Optical transmittance at 550 nm for a ~300-nm-thick $NiO_{1.15}$ film subjected to 500 CV cycles in the range 2.0–4.0 V, then placed in the electrolyte for 20 h without any applied potential, then doing 500 CV's again, subsequently applying a constant potential of 4.1 V for 20 h and finally performing 500 CV's.

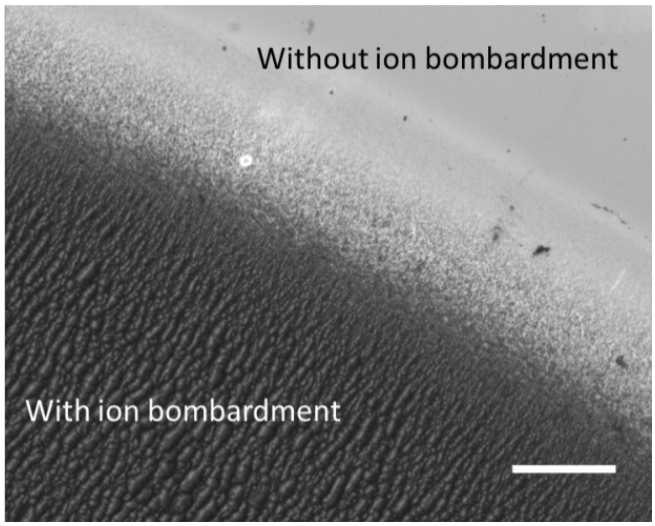

Figure S5. Optical micrograph of a ~300-nm-thick $NiO_{1.15}$ film. Dark and light areas show film morphologies with and without ion exposure inherent in the ToF-ERDA measurements, respectively. The scale bar is 100 µm.